

## **Physics Study of EC-Excited Current Generation via Current Jump in the Compact Plasma-Wall-Interaction Experimental Device**

T. Yoshinaga 1), K. Hanada 2), H. Zushi 2), K. Nakamura 2), K. N. Sato 2), H. Idei 2), M. Sakamoto 2), M. Hasegawa 2), T. Morisaki 1), Y. Nakashima 3), N. Nishino 4), M. Nagata 5), N. Fukumoto 5), Y. Takase 6), T. Maekawa 7), Y. Kishimoto 7), O. Mitarai 8), N. Yoshida 2), K. Tokunaga 2), Y. Hirooka 1), Y. Higashizono 2), S. Kawasaki 2), H. Nakashima 2), A. Higashijima 2), R. Bhattacharyay 2), S. Kawano 2), S. Kawakami 2), T. Kikukawa 2), K. Dono 2), M. Ishiguro 2), H. Honma 2), T. Miyazaki 2), T. Ryokai 2), T. Sakimura 2), Y. Inada 2), S. Watanabe 2) and Y. Wataya 2)

1) National Institute for Fusion Science, Toki, Japan

2) Kyushu University, Kasuga, Japan

3) University of Tsukuba, Tsukuba, Japan

4) Hiroshima University, Hiroshima, Japan

5) University of Hyogo, Himeji, Japan

6) The University of Tokyo, Kashiwa, Japan

7) Kyoto University, Kyoto, Japan

8) Kyushu Tokai University, Kumamoto, Japan

e-mail contact of main author: [yoshinaga.tomokazu@LHD.nifs.ac.jp](mailto:yoshinaga.tomokazu@LHD.nifs.ac.jp)

**Abstract.** Non-inductive current start-up experiments by using electron cyclotron heating and current drive (ECH/ECCD) technique has been conducted in the Compact Plasma-wall-interaction experimental Device (CPD), which is a small spherical tokamak device. By applying 8.2 GHz RF under steady external fields, plasma currents are generated and closed flux surface configurations are formed spontaneously. Two discharge modes are found. The first one is the “current jump” discharge, in which the closed flux configuration is formed via the rapid increase of the plasma current under relatively high vertical magnetic field. The second one is a slow current increase discharge under lower vertical field, in which the closed flux surfaces are formed during a slow current increase with the slow increase of microwave power. Since the higher plasma currents under higher vertical fields can be obtained only via the current jumps, the current jump phenomena seems to be essential for the non-inductive start-up scenario based on ECH/ECCD technique. By comparing the co-directional O-mode injection and the normal X-mode injection in the current jump discharges, the current jump occurred at lower RF power in the co-directional O-mode than that in the normal X-mode. However, the values of plasma current just before and after current jumps did not depend on the injection mode.

### **1. Introduction**

In toroidal systems plasmas are confined in the nested magnetic surface configurations. Especially in tokamak devices the magnetic surfaces must be generated and sustained by the toroidal plasma currents flowing in the plasmas themselves. The plasma currents are initiated by the ohmic heating (OH), which uses toroidal electric field induced by the central solenoid (CS) in conventional tokamak systems including ITER. In spherical tokamaks (STs), however, it is unlikely to place the large CS for the plasma current start-up because of their own shape, low-aspect-ratio, which originates all the advantages of the ST concept such as high  $\beta$ , high bootstrap current fraction, and reduced construction cost. Therefore, it is highly desirable to establish the alternative plasma current start-up scenario in STs and various methods are studied in various devices [1-6].

Electron cyclotron heating and current drive (ECH/ECCD) is potentially a possible candidate of the current start-up method, since it might be able to realize plasma initiation by EC-

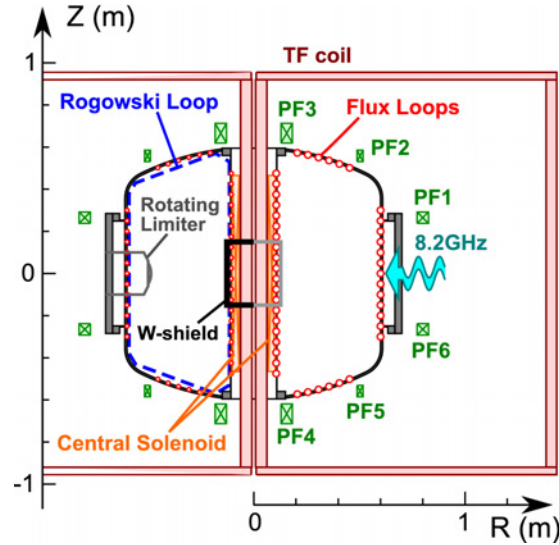


FIG. 1: The Schematics of CPD.

resonance (ECR) breakdown, current initiation and current ramp-up simultaneously by injecting microwaves from small antennas remote from the core plasma region. Recently, the “current jump” phenomena, which is a spontaneous increase of the plasma current accompanying the change of the field topology from the externally-applied open field structure to the closed flux structure, have been observed widely in EC-heated toroidal plasmas [1,4,7,8]. Moreover, further current ramp-up was also realized by increasing the external vertical field for toroidal equilibrium after the current jump in the LATE device [4]. While all these results suggest that the EC-based start-up scenario attractive, further understandings about current jump physics must be necessary to establish this scenario. The drastic and complex transitions must arise both in toroidal equilibrium conditions and particle confinements during the current jump phase. In this paper, we will present the results of the experiments conducted in the Compact Plasma-wall-interaction experimental Device (CPD) related to the current jump phenomena. In section 2, experimental setup is described. The experimental results are presented and discussed in section 3, and summarized in section 4.

## 2. Experimental Setup

Figure 1 shows the schematic of CPD. Both of the inner diameter and the height of the stainless-steel vacuum vessel are 1.2 m. The center post, whose outer diameter is 0.22 m, encloses four turns of toroidal field coils and CS. Around the mid-plane, it is covered by four pieces of quarter round tungsten-coated shield, the outer diameter and the height of which are 0.255 m and 0.3 m, respectively. There are three sets of vertical field coils (PF17, PF26 and PF35), which can be driven separately by the pre-programmed power supplies. The rotating drum limiter (RL) is installed for the active wall conditionings [9]. The RL head is placed at  $R = 0.48$  m in the experiments.

Microwave at 8.2 GHz from 8 klystrons is transmitted separately to the eight rectangular waveguide antennas and injected from the weak field side. Four antennas are placed for the injection of the wave vector normal to the field line and of the electric field inclined at  $22.5^\circ$  to the vertical ( $Z$ ) axis (we call this mode “X-mode” for simplicity). The remaining four antennas are used for the injection of the “O-mode”, which has the electric field orthogonal to

the X-mode. The waves in O-mode can be injected tangentially by the movable reflectors. The working gas is hydrogen. It is introduced into the vessel prior to the microwave injection. The typical filling gas pressure is  $\sim 10^{-3}$  Pa.

Plasma current is measured by the Rogowski coil installed on the vessel inner wall. Magnetic flux profiles are estimated from the 45 flux loop signals by using a similar technique to that mentioned in [10]. In addition, a lithium (Li) sheet beam imaging technique for density profile measurement [11,12], a H $\alpha$ -filtered high-speed (1 ms) camera [13], and an ultra-high-speed (25  $\mu$ s) camera are used to monitor the plasma shapes. Adding to these imaging diagnostics, 140 GHz interferometry, 6 - 20 GHz reflectometry, directional electrostatic probe diagnostics and spectroscopic measurements on H $\alpha$  and OII lines are conducted. H $\alpha$  line intensity is monitored along two lines of sight: one is a tangential chord which looks at the RL head tangentially on the mid-plane, and the other is an oblique chord which looks down at the lower part of the CS from the top port. The OII chord looks at the CS radially on the mid-plane.

### 3. Experimental Results

Two patterns of discharges are found in the CPD experiments. One is the current jump discharge, which are obtained under the relatively high vertical field ( $B_v \geq 3 \times 10^{-3}$  T). Figure 2 (a) - (e) shows a typical waveform of the discharge with current jump under a weakly mirror-shaped vertical field [see Fig. 2 (f)] with  $n$  (decay index) = 0.1 at  $B_v = 3.9 \times 10^{-3}$  G

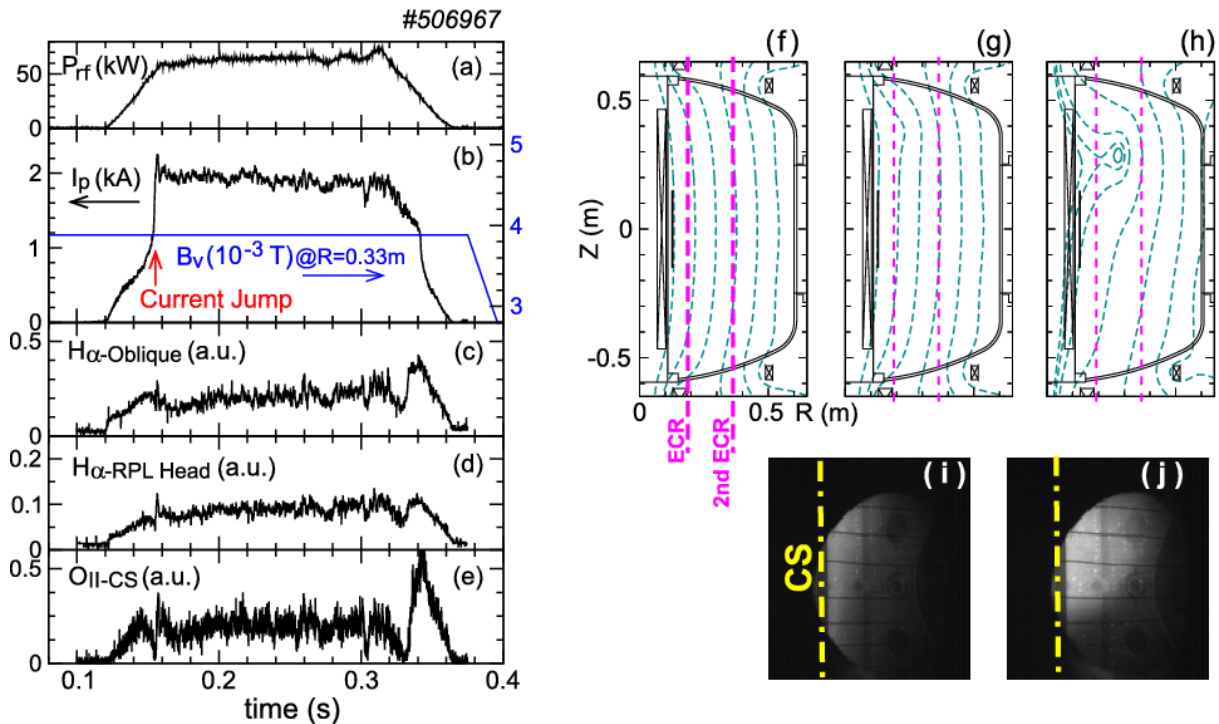


FIG. 2. Typical current jump discharge. (a) RF power, (b) plasma current and vertical field, (c) H $\alpha$  line intensity on the oblique chord, (d) H $\alpha$  line intensity on the tangential chord, and (e) OII line intensity on the radial chord. (f) - (h) Poloidal flux surfaces of (f) the externally applied vertical field, (g) just before current jump ( $t \sim 0.145$  s) and (h) just after current jump ( $t \sim 0.17$  s). (i), (j) H $\alpha$ -filtered images just before ( $t = 0.153$  s) and after ( $t = 0.157$  s) the current jump.

(both at  $R = 0.33$  m). During the low microwave power ( $\sim 1$  kW) injection phase before  $t = 0.12$  s, a thin cylindrical plasma is generated on the EC resonance (ECR) layer ( $B = 0.29$  T) at  $R = 0.19$  m. When  $P_{rf}$  starts to increase slowly at  $t = 0.12$  s, plasma current ( $I_p$ ) also starts to increase with  $P_{rf}$  as shown in Fig. 2 (a) and (b). When  $I_p$  reaches  $\sim 1$  kA under  $P_{rf} = 50$  kW at  $t = 0.154$  s,  $I_p$  turns into a rapid increase (current jump) and reaches  $\sim 2$  kA in  $\sim 3$  ms. After this current jump,  $I_p$  becomes constant until  $P_{rf}$  starts to decrease at  $t \sim 0.32$  s. Magnetic analysis shows that the open magnetic field structure just before current jump [Fig. 2 (g)] changes into the upward-shifted closed flux surface configuration during the current jump phase, as shown in Fig. 2 (h). The topological change coincides with the change in the  $H\alpha$ -filtered images as shown in Fig. 2 (i) and (j). The stepwise increase of  $H\alpha$  signal on the tangential chord is observed concurrently with the current jump as shown in Fig. 2 (d). This may reflect the radial enlargement of the plasma loop. The oblique  $H\alpha$  line and the radial OII line [Fig. 2 (c) and (e)] also suggest the topological change. The sheet Li beam measurement also confirms that the closed flux configurations are formed by the current jumps [12]. Moreover, it shows that the electron density exceeds the cutoff density of the incident EC-wave ( $8.3 \times 10^{17} \text{ m}^{-3}$ ). This suggests that the electron Bernstein wave heating is taking place.

In Fig. 3, the other discharge pattern under a lower  $B_v$  field ( $B_v = 2.9 \times 10^{-3}$  T) with  $n = 0.32$  [see Fig. 3 (f)] are shown. In this discharge pattern,  $I_p$  slowly increases with increase of  $P_{rf}$ , and current jump is not clearly observed as shown in Fig. 3 (a) and (b). Stepwise increases in the tangential  $H\alpha$  and the radial OII line intensities, which may be related with the topological change from open to closed structure, are observed at  $t \sim 0.14$  s [see Fig. 3 (d) and (e)]. The magnetic analysis showed that the closed flux surfaces are formed during this period as shown in Fig. 3 (g) and (h). While the change of the  $H\alpha$ -filtered image is very little in shape, the drastic increase of the intensity is observed as shown in Fig. 3 (i) and (j), and may indicate

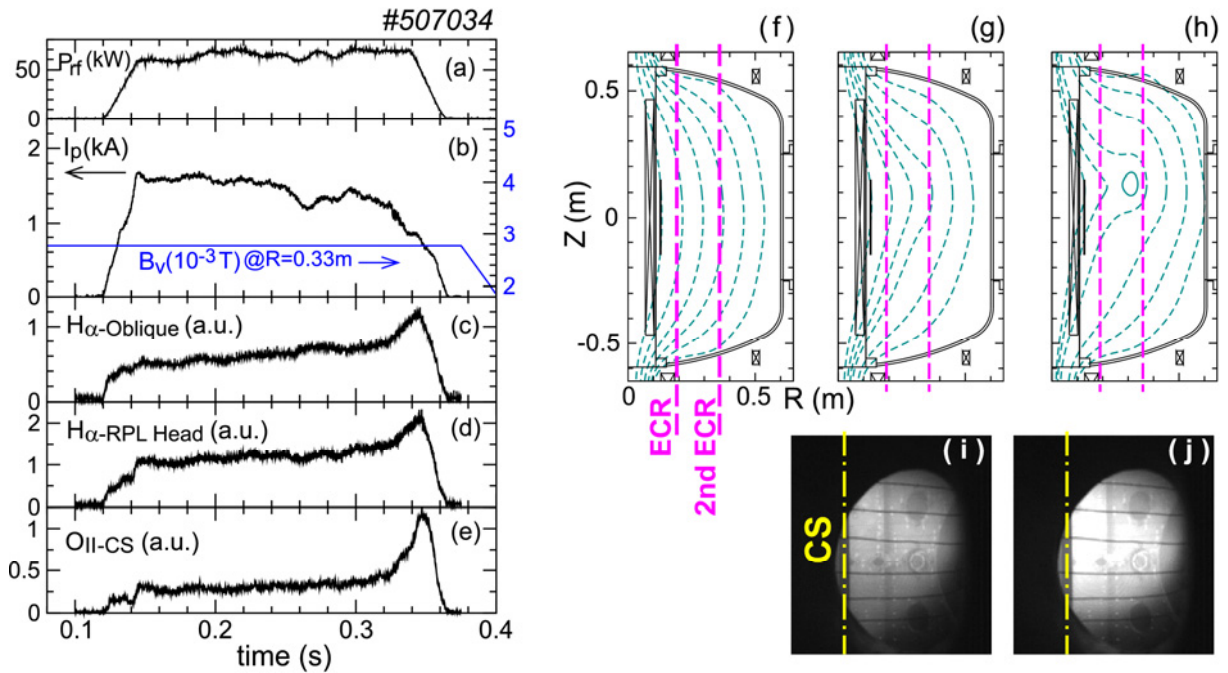


FIG. 3. Discharge without current jump. (a)  $P_{rf}$ , (b)  $I_p$  and  $B_v$ , (c)  $H\alpha$  on the oblique chord, (d)  $H\alpha$  on the tangential chord and (e) OII on the radial chord. (f) – (h) Poloidal flux structure of (f) the external field, (g) the field at  $t \sim 0.135$  s and (h) at  $t \sim 0.16$  s. (i), (j) The corresponding  $H\alpha$  images (i) at  $t = 0.138$  s and (j) at  $t = 0.146$  s.

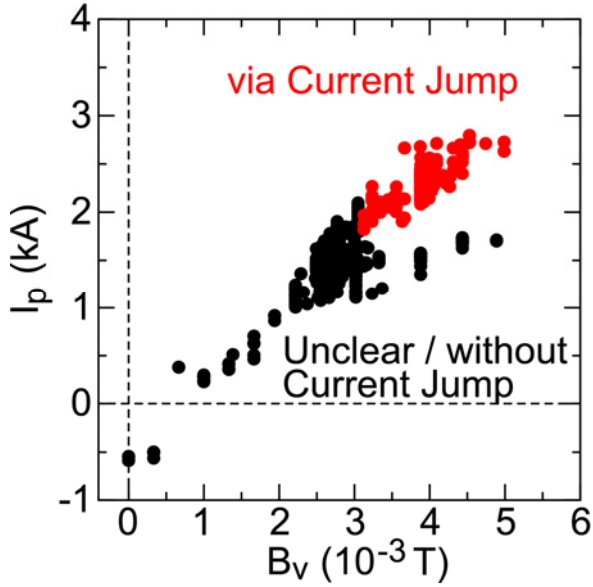


FIG. 4. Achieved  $I_p$  under various  $B_v$  fields.

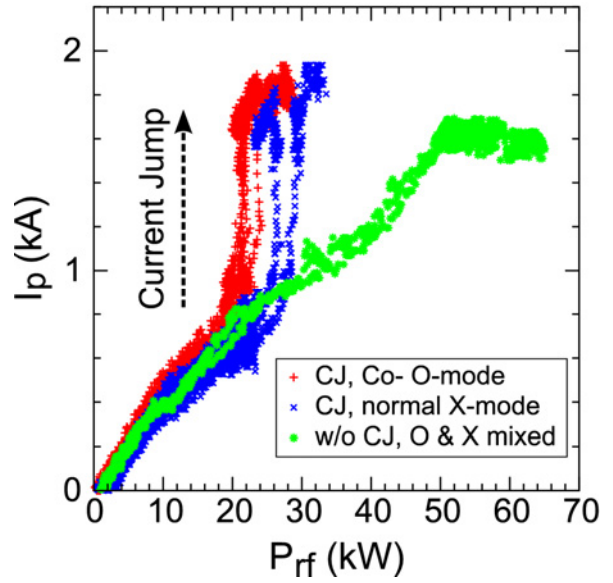


FIG. 5. Transient  $I_p$  vs.  $P_{rf}$  in the discharges with and without current jump (CJ). For CJ discharges, co-directional O-mode and normal X-mode are plotted.

the improvement of confinement by the formation of the closed flux surfaces. Larger LCFS structure with a suppressed vertical shift compared to the discharge in Fig. 2 is suggested by both the magnetic analysis and the  $H\alpha$  image. This may be because of the external  $B_v$  field with a somewhat stronger  $n$  as shown in Fig. 3 (f).

The values of  $I_p$  obtained under various  $B_v$  fields with  $P_{rf} \leq 60$  kW are plotted in Fig. 4. The maximum  $I_p$  under each given  $B_v$  tend to increase linearly with  $B_v$ . The ratio of increments in  $I_p$  and in  $B_v$  is  $dI_p/dB_v \sim 0.08$  kA/G, which is roughly similar to that obtained in the same scale STs, LATE and TST-2 [7,8]. Relatively high  $I_p$  ( $\geq 2$  kA) can be achieved only via current jumps under relatively high  $B_v$  ( $\geq 3 \times 10^{-3}$  T). Without current jump,  $I_p$  saturates at  $\sim 1.7$  kA in this  $B_v$  range. This shows that the current jump is essential to achieve the higher  $I_p$  under the higher  $B_v$  in the EC-based start-up scenario. Under lower  $B_v$  ( $\leq 3 \times 10^{-3}$  T) fields, on the other hand,  $I_p$  can reach the proportional level to  $B_v$  by the slow increase with  $P_{rf}$ . Some toroidal equilibrium condition may determine the achievable  $I_p$ .

Figure 5 shows the transient values of  $I_p$  plotted against the transient  $P_{rf}$  in the discharges with and without current jump. For the current jump discharges, the co-directional O-mode injection and the normal X-mode injection are compared under the same  $B_v$  field condition with the discharge shown in Fig. 2 ( $B_v = 3.9 \times 10^{-3}$  T and  $n = 0.1$  at  $R = 0.33$  m). The co- O-mode injection turned out to be more effective than the normal X-mode, in the sense that the threshold level of  $P_{rf}$ , at which the current jump starts, is lower in the co-directional O-mode ( $P_{rf} \sim 20 - 23$  kW) than in the normal X-mode ( $P_{rf} \sim 26 - 29$  kW). Meanwhile, the value of  $I_p$  just before current jump is almost identical in both modes. This suggests that the critical parameter for current jump occurrence should be  $I_p$  itself and therefore the poloidal magnetic field structure. The current generation mechanism in the current jump phase may be related to this, since the mechanism is considered to be originated from the asymmetric confinement of

fast electrons in the velocity space [7,14], which depends on the magnetic field structure. The characteristics of  $I_p$  vs.  $P_{rf}$  is similar between the two modes before current jump, while the co- O-mode is slightly more effective than the normal X-mode. Moreover, the case without current jump which is shown in Fig. 3 ( $B_v = 2.9 \times 10^{-3}$  T and  $n = 0.32$  at 0.33 m) also has the similar characteristics when  $P_{rf}$  is low ( $\leq 20$  kW). It is understood that the plasma current under such open field configuration is generated by the pressure-driven-current mechanism [15]. Since  $I_p$  is proportional to the plasma pressure, linear increase of  $I_p$  with  $P_{rf}$  may be related to the linear increase of electron pressure with  $P_{rf}$  under open configuration.

By comparing the discharges with and without current jump, current jump discharge turned out to be advantageous since higher  $I_p$  can be achieved with lower  $P_{rf}$  injection. The difference between these two discharge modes might arise from the current generation mechanism. Under lower  $B_v$  fields, the pressure-driven-current can be large since it is inversely proportional to  $B_v$  [15], and might become dominant. In this situation, it may be necessary to increase  $P_{rf}$  in order to raise the electron pressure and  $I_p$  to the proportional level to the external  $B_v$ . Meanwhile, asymmetric confinement mechanism might become dominant since higher energy electrons can be confined and the pressure-driven-current becomes lower under higher  $B_v$  fields. When the poloidal field structure is deformed to a certain level by the self-field of the pressure-driven-current, the energetic electrons in the current-carrying direction become confined, then the current jump may be turned on. The RF power in this situation is required only to raise the electron pressure to the level that the deformations of the external  $B_v$  fields by the self-field of the pressure-driven-current can enhance the confinement asymmetry. The value of  $P_{rf}$  for this may be lower than that required to form closed field equilibria under lower  $B_v$  fields.

#### 4. Summary

Non-inductive current generation and formation of closed flux configuration are demonstrated in CPD. There are two patterns of discharge: one is the current jump discharge under relatively higher  $B_v$  field ( $\geq 3 \times 10^{-3}$  T), and the other is the discharge with slow current increase under lower  $B_v$  field ( $\leq 3 \times 10^{-3}$  T). Current jump discharge turned out to be effective in achieving the higher  $I_p$  ( $\geq 2$  kA) under the higher  $B_v$  with relatively low  $P_{rf}$  ( $\sim 20 - 30$  kW) injection compared to the slow increase discharge. The threshold  $P_{rf}$  level, at which the current jump starts, became lower in the co-directional O-mode injection than in the normal X-mode injection.

The threshold  $P_{rf}$  level for current jump occurrence might be related to the RF power density, since it may be related to the poloidal field deformation by the pressure-driven-current, which is proportional to the plasma pressure. According to the results in CPD, the critical power density becomes  $\sim 25$  kW/m<sup>3</sup>. In the Q-shu University Experiment with Steady State Spherical Tokamak (QUEST) [16], which is a double-sized ST and starts to operate this year, the power density becomes similar to this value when  $P_{rf} \sim 200$  kW is injected. This is the typical level in the QUEST experimental plan. Moreover, EC-wave launching system based on the phased-array-antenna technique [17], which enables wave injection in arbitral modes and angles, will be installed aiming the effective electron Bernstein wave heating and current drive.

## Acknowledgment

This work was performed with the support and under the auspices of the NIFS Collaboration Research Program (NIFS05KUTR007).

## References

- [1] GRYAZNEVICH M., et al., Nucl. Fusion **46** (2006) S573.
- [2] RAMAN R., et al., Nucl. Fusion **47** (2007) 792.
- [3] TAKASE Y., et al., Nucl. Fusion **46** (2006) S598.
- [4] MAEKAWA T., et al., Nucl. Fusion **45** (2005) 1439.
- [5] NAGATA M., et al., Phys. Plasmas **10** (2003) 2932.
- [6] MITARAI O., et al., J. Plasma Fusion Res. **80** (2004) 549.
- [7] YOSHINAGA T., et al., Phys. Rev. Lett. **96** (2006) 125005.
- [8] SUGIYAMA J., et al., Plasma and Fusion Research **3** (2008) 026.
- [9] ZUSHI H., et al., “Active Particle Control Experiments and Critical Particle Flux Discriminating between the Wall Pumping and Fueling in the Compact Plasma wall interaction Device CPD Spherical Tokamak”, this conference.
- [10] YOSHINAGA T., et al., Nucl. Fusion **47** (2007) 210.
- [11] BHATTACHARYAY R., et al., Physics of plasmas **15** (2008) 022504.
- [12] KIKUKAWA T., et al., Plasma and Fusion Research **3** (2008) 010.
- [13] HIGASHIZONO Y., et al., submitted to Rev. Sci. Instrum.
- [14] EJIRI A. et al., Nucl. Fusion **47** (2007) 403.
- [15] FOREST C.B., et al., Phys. Plasmas **1** (1994) 1568.
- [16] HANADA K., et al., “Physical Design of MW-class Steady-state Spherical Tokamak, QUEST”, this conference.
- [17] IDEI H., et al., “Ray Trace and Fokker-Plank Analysis for Electron Bernstein Wave Heating and Current Drive in QUEST”, International Congress on Plasma Physics 2008, BEH-P2-157.